Polymer 51 (2010) 4663–4666

Contents lists available at ScienceDirect

Polymer

journal homepage: www.elsevier.com/locate/polymer

Polymer Communication

Asymmetric morphology from an organic/organometallic block copolymer

Muruganathan Ramanathan [a], Joseph Strzalka [b], Jin Wang [b], Seth B. Darling [a,*]

[a] Center for Nanoscale Materials, Argonne National Laboratory, Argonne, IL 60439, United States
[b] X-ray Science Division, Argonne National Laboratory, Argonne, IL 60439, United States

ARTICLE INFO

Article history:
Received 4 June 2010
Received in revised form
3 August 2010
Accepted 8 August 2010
Available online 14 August 2010

Keywords:
Block copolymer
Polymer materials
Self-assembly

ABSTRACT

Block copolymer self-assembly is a burgeoning subject in polymer and materials science driven by both fundamental and applied inspirations. Whereas the vast majority of block copolymer studies have focused on highly symmetric morphologies, here we report the first observation of an unusual asymmetric cylindrical phase in thick films of an organic/organometallic block copolymer, poly(styrene-*block*-ferrocenyldimethylsilane) (PS-*b*-PFS). Microscopy and X-ray scattering data establish the lack of symmetry in this structure and reveal an unusual 3-D network organization. Following selective removal of the PS matrix, the remaining nanoporous film has characteristics of potential value in separation applications such as substantial interconnection (mechanical strength), uniform pore size, and chemical and physical stability.

1. Introduction

Block copolymers (BCPs) have been the subject of escalating attention over the past decade both driven by fundamental polymer science issues and, increasingly, by potential applications ranging from optoelectronics to separations to information technology [1–7]. BCPs are exciting materials because they tend to self-assemble into a variety of ordered morphologies in which both the periodic length scale and the topology can be tuned through synthetic chemical design of the constituent macromolecules.

The standard phase diagram for a coil–coil diblock (comprised of two flexible blocks, A and B) copolymer consists of four microphase-separated morphologies: spheres, cylinders, gyroids, and lamellae [8]. (Note that BCPs containing more than two blocks can exhibit far more complex phase diagrams [9].) Morphology is determined by a combination of the relative volume fraction of the two blocks and the interaction between the blocks as quantified by the product of the Flory-Huggins parameter and the molecular weight. Several additional phases have been reported in the literature, such as the plumber's nightmare [10] and perforated lamellae [11], among others; these structures generally represent kinetically trapped states rather than thermodynamic equilibria, though they can be remarkably stable in actuality. In all cases, however, this set of morphologies exhibits relatively high symmetry.

Recently, a new morphology has been added to this collection: an asymmetric phase that resembles a combination of in-plane and perpendicular cylinders with many juncture nodes [12,13]. This phase has been observed in only a few polymer systems to date, namely poly(styrene-*block*-4-vinylpyridine) (PS-*b*-P4VP) and poly(styrene-*block*-methyl methacrylate) (PS-*b*-PMMA), both fully organic systems. In the case of PS-*b*-P4VP, this unusual phase was only observed following a phase-inversion process, which uses a sequential non-solvent/solvent treatment. Pores formed as a result of competition between non-solvent-induced phase separation and the self-assembly of the BCPs. The pores represent the volume that was occupied with water prior to drying and are lined by P4VP domains within a PS matrix. Structural disorder is a result of the dominant role played by the precipitation of the BCP from solution with respect to the microphase separation process.

The PS-*b*-PMMA asymmetric phase formation mechanism is qualitatively different. In this case, the mixture of cylinders oriented parallel and perpendicular to the film plane is the result of the relatively large film thickness (~160 nm) with respect to the domain periodicity (~12 nm). The film-substrate and film–air interfaces both induce a perpendicular orientation, but the driving force weakens further from these interfaces, thereby permitting other orientations to coexist with the perpendicular orientation. Once the asymmetric morphology forms, the PMMA phase can be selectively removed by a UV/acetic acid treatment, leaving behind a nanoporous film. Because of the substantial mechanical strength afforded by the three-dimensional interconnectedness of this phase [14], films of the asymmetric structure have shown great promise in nanofiltration applications [13].

* Corresponding author. Tel.: +1 630 252 4580; fax: +1 630 252 4646.
E-mail address: darling@anl.gov (S.B. Darling).

0032-3861/$ – see front matter © 2010 Elsevier Ltd. All rights reserved.
doi:10.1016/j.polymer.2010.08.012

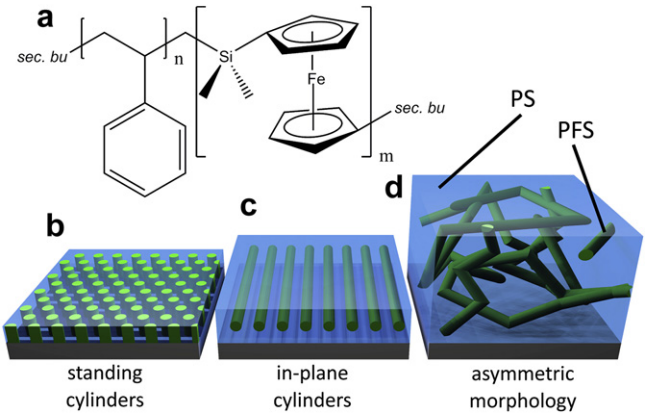

Fig. 1. (a) Chemical structure of PS-*b*-PFS block copolymer; (b–d) Schematics of film morphology progression with film thickness, ranging from standing cylinders to in-plane cylinders to the new asymmetric structure as the thickness increases.

We have recently reported on the thickness-dependent morphology of a cylinder-forming poly(styrene-*block*-ferrocenyldimethylsilane) (PS-*b*-PFS) BCP (Fig. 1a) [15,16]. This polymer is an organic/organometallic hybrid, and this affords it some physical and chemical properties unlike its fully organic brethren [17–20]. For example, there is a substantial differential etch resistance between these two blocks, which is an important advantage in lithography applications [21,22], where the domains are typically well ordered. Moreover, when the organic block is selectively removed, the remaining material is highly impervious to various chemical environments and is thermally more stable than typical polymeric systems. This could be a critical benefit for industrial separation applications. Unlike classic cylinder-forming BCPs, this particular PS-*b*-PFS material exhibits a transition from cylinders oriented perpendicular to the film plane to cylinders parallel to the plane as the film thickness is varied (Fig. 1b and c). Herein, we report on an additional phase change that occurs at still greater film thicknesses, where an asymmetric phase appears (Fig. 1d). We believe this is the first observation of such a phase in an organic/organometallic BCP.

2. Experimental

PS-*b*-PFS with a molecular weight of 90,000 g mol^{-1} (M_n = 60,000 PS/30,000 PFS) and a polydispersity index of 1.2 was obtained from Polymer Source as a custom synthesis and used as received. Thin films were spin-cast at various speeds (1000–5000 rpm) from toluene solutions with concentrations ranging from 0.25 to 5.0 wt.-% onto clean Si_3N_4 substrates. Thick films were prepared by drop casting from the 5.0 wt.-% solution. Thermal annealing was carried out under an inert Argon atmosphere at 140 °C. Film thicknesses were measured with a Filmetrics F20 ellipsometer calibrated by comparison with scratched samples imaged with atomic force microscopy (AFM). As deposited, the thick glassy PS layer present at the surface makes imaging microphase-separated domains difficult, therefore, prior to imaging the PS phase was removed using oxygen reactive ion etching. Oxygen reactive ion etching (RIE) was performed in a March CS-1701 at a pressure of 100 m Torr, power of 20 W, oxygen flow rate of 7 sccm, and an etch time of 3 min. AFM imaging was performed with a Veeco MultiMode V system equipped with active vibrational isolation and using Veeco tapping-mode etched silicon probes. TEM bright field imaging was performed using a 300 kV FEI Tecnai F30 microscope. Silicon nitride membrane substrates for TEM were obtained from SPI Supplies. Field-emission scanning electron microscopy (SEM) imaging was performed with a JEOL JSM7500F microscope.

Grazing incidence small-angle X-ray scattering (GISAXS) measurements were conducted at beamline 8-ID-E of the Advanced Photon Source, Argonne National Laboratory. The X-ray beam, 100 microns wide and 50 μm high with an energy of 7.35 keV (λ = 1.687 Å), impinges on the sample with incident angle α and is scattered into a MAR165 CCD-based detector positioned at a distance approximately 2 m from the sample. Data were collected over a range of incident angles and exposure times up to 100 s with different sized beamstops to block the most intense parts of the incident and scattered radiation. The sample and flight paths are maintained under vacuum. Further details of the setup were as described previously [23]. Because of the strong contrast between the organic and organometallic blocks, it was not necessary to remove the PS domains prior to collecting GISAXS data.

3. Results and discussion

Film thickness appears to be the dominant factor determining the morphology exhibited in the PS-*b*-PFS films [16]. It is perhaps more useful to refer to the thickness in the context of the characteristic domain periodicity length scale, which for the specific polymer studied here is ~70 nm. When the film thickness is significantly thinner than this value, <45 nm, standing cylinders are

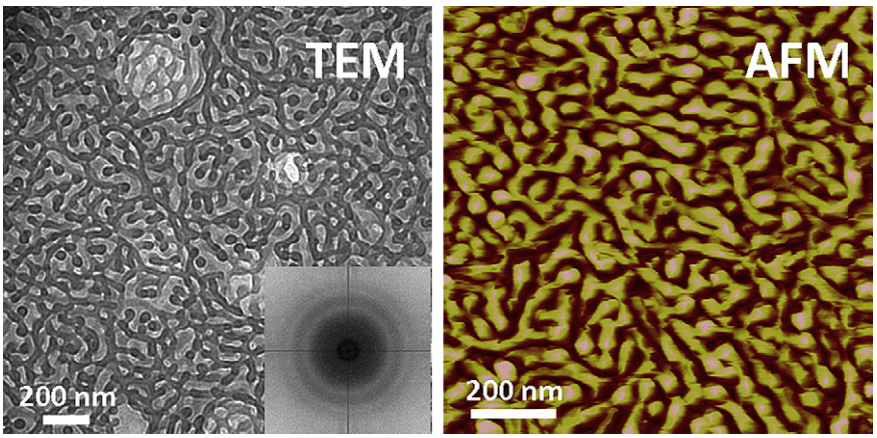

Fig. 2. Bright-field TEM and tapping-mode AFM phase images of the asymmetric morphology for films of ~120 and 250 nm thickness, respectively. Both images are obtained from films from which the PS phase has been selectively removed using RIE so only the (RIE-modified) PFS phase remains. The inset on the TEM image is a 2-D Fourier transform of this image exhibiting circular rings.

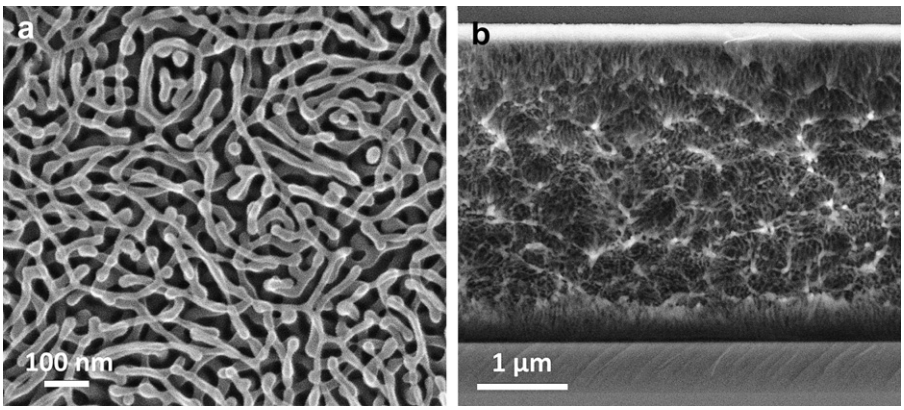

Fig. 3. SEM top-view (a) and cross-sectional (b) images of the asymmetric morphology for a film of ~3 μm thickness. Both images are obtained from a film from which the PS phase has been selectively removed using RIE so only the (RIE-modified) PFS phase remains. The cross-sectional view shows how the orientation of cylindrical domains varies through the thickness of the film.

observed, perhaps due to entropic effects [24] or to the influence of solvent evaporation during the spin casting process. This structure transitions to the more traditional in-plane cylinders as the film thickness becomes comparable to the domain periodicity, ~50–70 nm, as a result of selective wetting of the interfaces with the PS block. Films thicker than 70 nm, however, display a wholly different morphology. Prior to imaging, the PS domains are removed using RIE, so the observed features represent only the minority PFS structure, which was originally embedded in a matrix of PS.

As observed with both transmission electron microscopy (TEM) and atomic force microscopy (AFM), the cylindrical PFS features adopt a mixture of these two orientations with a substantial degree of interconnection (Fig. 2). Whereas the AFM image is difficult to interpret by itself, when viewed together with the TEM data, it is clear that this morphology is in actuality a 3-D network of cylinders. There is no apparent symmetry to this structure, though it can be difficult to discern symmetric structures when viewing micrographs. Searching for symmetry is often more straightforward in reciprocal space, obtained by performing a 2-D Fourier transform (FT) on the images to shift to the frequency domain. As seen in the inset in Fig. 2, a discrete FT of the TEM image reveals a series of concentric circular rings. These rings indicate that there is a characteristic periodicity in the image, which in this case is rooted in the self-assembled microphase-separated structure. As the intensity of the rings is circularly symmetric, there does not appear to be any preferential orientation to the cylinders, that is, the phase seems to be asymmetric.

The asymmetric phase is observed in all films above a certain thickness, suggesting it reflects the bulk morphology of this polymer, as evidenced by the scanning electron micrographs of a ~3 μm-thick film depicted in Fig. 3. While the top surface is structurally similar to that presented in the micrographs in Fig. 2, cross-sectional imaging reveals the three-dimensional nature of the asymmetric phase. In this film, the orientation of cylindrical PFS microdomains varies through the layer thickness.

A complementary measurement to the real space data presented above is GISAXS, which provides reciprocal space analysis of the film structure. Data from a typical sample with the asymmetric morphology appear in Fig. 4a. The peaks at $q_y = 0.125\ \mathrm{nm}^{-1}$ indicate electron density contrast present in the unetched sample at a length scale of 50 nm, consistent with the length scale observed in the micrographs. There is a weak second order peak but no higher order peaks, demonstrating the lack of symmetry in the sample.

Considering the two formation mechanisms reported for asymmetric cylindrical phases in other BCP materials, the scenario that applies to the PS-*b*-PFS system under consideration here is clearly more analogous to that reported for thick PS-*b*-PMMA films. In the absence of phase-inversion pathways, explanations for the atypical 3-D network structure must lie in other aspects of the self-assembly process. In fact, the asymmetric morphology may actually not be as atypical as one might conclude from its relative scarcity in the literature. Most BCP studies focus on either ultrathin films or bulk and solution-based materials. In both the PS-*b*-PMMA case reported by Kim et al. [13]. and the PS-*b*-PFS system reported here, the thick film regime, in contrast, was found to be critical for the formation of the asymmetric phase. Additional studies with cylinder-forming BCPs in this thickness range may yield similar results. The lack of symmetry is likely evidence for the metastability

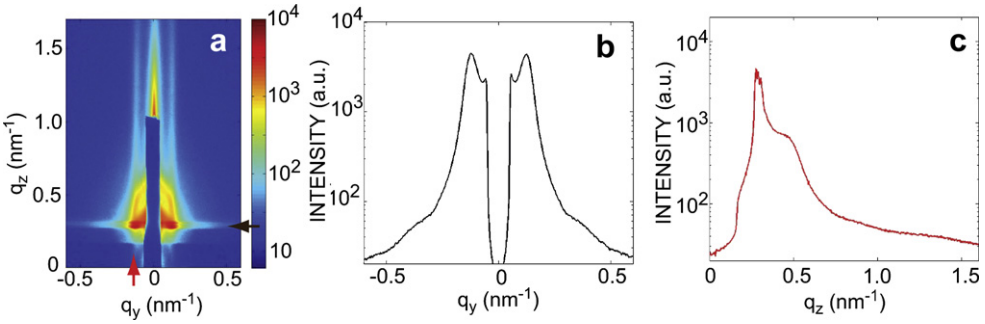

Fig. 4. GISAXS data from a thin film sample exhibiting the asymmetric morphology ($\alpha = 0.210°$, 10 s exposure) with intensity represented on a logarithmic color scale (a). Colored arrows indicate where the linecuts in (b) and (c) were taken. Only first-order peaks (at $q_y = 0.125\ \mathrm{nm}^{-1}$) and weak second order peaks appear in these data due to the lack of symmetry of this phase. Longer exposures do not show any additional features.

of these structures, meaning that the processing plays an important role in the structure formation. The global minimum energy structure is presumably a more ordered arrangement in which the orientation of the cylindrical domains is more uniform, perhaps with grain boundaries near the interfaces depending on the interfacial energies. The relatively large molecular weight ($M_w = 90{,}000$) of the polymer studied here facilitates the formation of metastable structures because the large scale reorganization of the chains is inhibited by substantial entanglement. We find that the asymmetric morphology persists following extensive thermal and/or solvent annealing. Some competition between parallel and perpendicular orientations is the expected source of the asymmetry. This competition emerges when the film thickness is large enough to diminish the role of interfacial effects, which are dominant in ultrathin films. Indeed, the regions near the interfaces exhibit greater orientational order than the interior of the film, as seen in Fig. 3b.

Within the context of filtration applications, it is important to consider the robustness of the membrane against harsh chemical or physical conditions. When PS-*b*-PFS is treated with oxygen RIE, the PS phase is completely degraded, but the PFS phase exhibits remarkable stability. Indeed, we have found it difficult to remove the residual PFS material following RIE exposure. Common solvents have no apparent effect—even with sonication—and thermal stability far exceeds that of organic polymers. The RIE-modified PFS material requires extremely aggressive treatment, such as extended exposure with Piranha solution, to remove it. The iron and silicon moieties in the PFS block undergo conversion in the RIE process to a Fe/Si oxide [25]. Separation membranes fabricated from this material can, therefore, be expected to display favorable stability.

4. Conclusions

An asymmetric cylindrical phase, previously only reported for a few organic BCP systems, has been observed in an organic/organometallic BCP. This morphology, which can be viewed as a mixture of in-plane and perpendicular cylinder orientations, is seen in films thicker than the characteristic cylinder domain periodicity. The proposed mechanism guiding the assembly of this structure is a confluence of competing driving forces for parallel and perpendicular orientations and the low chain mobility afforded by the high molecular weight of the BCP. When the film is treated with RIE, the PS matrix is removed and the remaining PFS network is chemically modified to become a robust Fe–Si oxide. Because of the combination of relatively monodispersed pore size, 3-D interconnection, and chemical/physical inertness, these films are potentially useful in mesoscale separation applications.

Acknowledgments

We thank V. Joshi for assistance with acquiring cross-sectional SEM images. Use of the Center for Nanoscale Materials and the Advanced Photon Source was supported by the U.S. Department of Energy, Office of Science, Office of Basic Energy Sciences, under contract No. DE-AC02-06CH11357.

References

[1] Cheng JY, Ross CA, Smith HI, Thomas EL. Templated self-assembly of block copolymers: top-down helps bottom-up. Adv Mater 2006;18:2505–21.
[2] Park C, Yoon J, Thomas EL. Enabling nanotechnology with self assembled block copolymer patterns. Polymer 2003;44:6725–7032.
[3] Tao Y, Ma B, Segalman RA. Self-assembly of rod-coil block copolymers and their application in electroluminescent devices. Macromolecules 2008;41:7152–9.
[4] Darling SB. Directing the self-assembly of block copolymers. Prog Polym Sci 2007;32:1152–204.
[5] Darling SB. Block copolymers for photovoltaics. Energy Environ Sci 2009;2:1266–73.
[6] Botiz I, Darling SB. Optoelectronics using block copolymers. Mater Today 2010;13:42–51.
[7] Balazs AC, Emrick T, Russell TP. Nanoparticle polymer composites: where two small worlds meet. Science 2006;314:1107–10.
[8] Bates FS, Fredrickson GH. Block copolymers—designer soft materials. Phys Today 1999;52:32–8.
[9] Chen H-Y, Fredrickson GH. Morphologies of ABC triblock copolymer thin films. J Chem Phys 2002;116(3):1137–46.
[10] Finnefrock AC, Ulrich R, Toombes GES, Gruner SM, Wiesner U. The plumber's nightmare: a new morphology in block copolymer-ceramic nanocomposites and mesoporous aluminosilicates. J Am Chem Soc 2003;125:13084–93.
[11] Zhu L, Huang P, Cheng SZD, Ge Q, Quirk RP, Thomas EL, et al. Dislocation-controlled perforated layer phase in a PEO-b-PS diblock copolymer. Phys Rev Lett 2001;86(26):6030–3.
[12] Peinemann K-V, Abetz V, Simon PFW. Asymmetric superstructure formed in a block copolymer via phase separation. Nat Mat 2007;6:992–6.
[13] Yang SY, Park J, Yoon J, Ree M, Jang SK, Kim JK. Virus filtration membranes prepared from nanoporous block copolymers with good dimensional stability under high pressures and excellent solvent resistance. Adv Func Mater 2008;18:1371–7.
[14] Young WC, Budynas RG. Roark's formulas for stress and strain. 7th ed. McGraw-Hill; 2002.
[15] Ramanathan M, Darling SB. Thickness dependent hierarchical meso/nano scale morphologies of a metal-containing block copolymer thin film induced by hybrid annealing and their pattern transfer abilities. Soft Matter 2009;5:4665–71.
[16] Ramanathan M, Nettleton E, Darling SB. Simple orientational control over block copolymer domains for etch mask applications. Thin Solid Films 2009;517:4474–8.
[17] Lammertink RGH, Hempenius MA, Thomas EL, Vancso GJ. Periodic organic-organometallic microdomain structures in poly(styrene-block-ferrocenyldimethylsilane) copolymers and blends with corresponding homopolymers. J Polym Sci Part B Polym Phys 1999;37:1009–21.
[18] Rider DA, Cavicchi KA, Power-Billard KN, Russell TP, Manners I. Diblock copolymers with amorphous atactic polyferrocenylsilane blocks: synthesis, characterization, and self-assembly of polystyrene-block-poly(ferrocenylethylmethylsilane) in the bulk state. Macromolecules 2005;38:6931–8.
[19] Lu J, Chamberlin D, Rider DA, Liu M, Manners I, Russell TP. Using a ferrocenylsilane-based block copolymer as a template to produce nanotextured Ag surfaces: uniformly enhanced surface enhanced Raman scattering active substrates. Nanotechnology 2006;17:5792–7.
[20] Gaedt T, Ieong NS, Cambridge G, Winnik MA, Manners I. Complex and hierarchical micelle architectures from diblock copolymers using living, crystallization-driven polymerizations. Nat Mat 2009;8:144–50.
[21] Lammertink RGH, Hempenius MA, van den Enk JE, Chan VZ-H, Thomas EL, Vancso GJ. Nanostructured thin films of organic-organometallic block copolymers: one-step lithography with poly(ferrocenylsilanes) by reactive ion etching. Adv Mater 2000;12:98–103.
[22] Cheng JY, Ross CA, Thomas EL, Smith HI, Vancso GJ. Fabrication of nanostructures with long-range order using block copolymer lithography. Appl Phys Lett 2002;81(19):3657–9.
[23] Li X, Narayanan S, Sprung M, Sandy A, Lee DR, Wang J. Developing a dedicated GISAXS beamline at the APS. AIP Conf Proc 2007;879:1387–90.
[24] Wang Q, Nealey PF, de Pablo JJ. Monte Carlo simulations of asymmetric diblock copolymer thin films confined between two homogeneous surfaces. Macromolecules 2001;34:3458–70.
[25] Lammertink RGH, Hempenius MA, Chan VZ-H, Thomas EL, Vancso GJ. Poly(ferrocenyldimethylsilanes) for reactive ion etch barrier applications. Chem Mater 2001;13:429–34.